DOI: 10.21062/mft.2024.072 http://www.journalmt.com

Design and Simulation of Secondary Acceleration Type Rotor for Vertical Shaft Impact Crusher

Canhui Wu (0009-0008-8314-1664), Limei Zhao (0000-0002-7718-8756), Cheng Zhang (0009-0009-3886-3358)
School of Mechanical Engineering, Guizhou University, Guiyang, China. Corresponding author's E-mail: lmzhao@gzu.edu.cn

In order to improve the crushing effect of the rotor of vertical shaft impact crusher on the particle, the design method of secondary accelerated rotor based on kinematics theory is proposed. And the operation effect of the secondary acceleration type rotor was verified using a combination of computational fluid dynamics and discrete element method (CFD-EDM). First, the kinematics of the particles thrown by the rotor throwing head was analyzed. On this basis, the structure of the secondary acceleration type rotor was designed by comprehensively considering factors such as the motion, friction, and collision recovery coefficient of particles; Then, based on the gas-solid coupling analysis method, a simulation model of the rotor's effect on particle acceleration was established and the reliability of the model was verified; Finally, the CFD-EDM method was used to calculate and analyze the motion process of particles in the crushing chamber, the collision position of particles in the crushing chamber, and the average throwing speed of the rotor. Research results show that roughly 77.6 % of the particles in the crushing chamber will collide with the impact plate to achieve secondary acceleration; The average throwing speed of the traditional rotor is 57.14 m/s, and the average throwing speed of the designed secondary accelerated rotor is 60.89 m/s, which is about 6% higher than the average throwing speed compared with the traditional rotor, and achieves the expected design purpose.

Keywords: Vertical shaft impact crusher, Secondary accelerated rotor, Kinematic analysis, CFD-DEM

1 Introduction

Because the vertical shaft impact crusher has the characteristics of good granularity, small size and low operating cost, etc., it has become an increasingly widely used production equipment in the industries of mineral grinding, metallurgy and construction aggregate processing [1-3]. The rotor of a vertical impact crusher is a key component for achieving particle crushing. The particle gains kinetic energy through the acceleration effect of the rotor, and after obtaining kinetic energy, the particle is thrown out at high speed from the rotor body, and then collides strongly with the cutting board of the crushing chamber to achieve crushing [4-7]. The better the acceleration effect of the rotor on the particle, the greater the kinetic energy obtained by the particle, and the better the crushing effect of the particle [8]. It can be seen that the structural form and parameters of the rotor have a crucial impact on the working efficiency of the crusher and the quality of the crushed products. Therefore, improving the structural form of the rotor of the vertical shaft impact crusher to achieve better acceleration effect on particles is a research work with theoretical and engineering practical significance.

In terms of the structural design of the rotor of a vertical shaft impact crusher, domestic and foreign scholars have conducted many research works to improve the particle acceleration effect of the rotor, and have achieved certain research results. The research results of Yaqoub et al. indicate that if the speed of the particle after the first impact crushing is used for the second impact crushing, the particle can save up to 50 % energy during the crushing process [9]. Zanden et al. studied the two acceleration processes and the trajectory of the particle in a synchronous impact crusher, and the results showed that the re-acceleration of the particle gives the crusher significant advantages in terms of energy saving, service life and production [10]. Li et al. found through discrete element simulation that when the number of guide plates and impact plates in a vertical shaft impact crusher is 5, the average throwing speed of the rotor is the highest [11]. Djordjevic et al. designed a new type of vertical axis impact crusher and studied its throwing law. They used simulation experiments to discuss the influence of the installation angle of the impact plate on the throwing speed [7, 8, 12, 13].

However, although some scholars have explored the issue of secondary acceleration of particles in the above studies, the research is limited to discussing the impact of secondary acceleration on the speed of throwing particles, and there is no in-depth analysis of the design method of secondary acceleration type rotors from a kinematic perspective. And the research is

based on multiple idealized assumptions, without considering the influence of factors such as friction between the particle and the guide plate, and the recovery coefficient of collision between the impact plate and the particle. Therefore, based on kinematic theory and considering factors such as friction of particles, this article analyzes the motion of particles thrown out by the throwing head, and proposes a design method for a secondary acceleration type rotor; Then, a simulation model of the acceleration effect of the rotor on the particle was established and the reliability of the model was verified; On this basis, the CFD-EDM method was used to calculate and analyze the motion process of the particle in the crushing chamber, the collision position of the particle in the crushing chamber, and the average throwing speed of the secondary acceleration type rotor. The operation effect of the secondary acceleration type rotor was verified, which has certain theoretical and engineering practical significance.

2 Improved design of rotor structure

In order to achieve better crushing effect of particles, the application enterprises of vertical shaft impact crushers often adjust the traditional rotor speed to a large value to enable the particles to obtain greater impact kinetic energy. However, research has shown that increasing the rotor speed can only improve the crushing effect of particles within a certain range. At the same time, increasing the rotor speed will have higher requirements for its dynamic balance, spindle bearings, and manufacturing quality. Moreover, excessive rotor speed will also cause a series of problems such as high energy consumption in the crushing process and poor particle size distribution of the crushed products [13-14].

In response to the above issues, this article takes the traditional rotor of the PL840 vertical shaft impact crusher produced by a certain enterprise (as shown in Figure 1 (a)) as the design basis, and designs a new type of rotor - a secondary acceleration type rotor, as shown in Figure 1 (b), which mainly includes a rotor body, a guide plate, a dividing cone, and an impact plate. During the crushing process, there are two acceleration processes: The particles that fall vertically from the feeding port onto the dividing cone are uniformly dispersed onto each guide plate by the high-speed rotating dividing cone. Subsequently, under the action of external forces such as friction and centrifugal force, the particles accelerate along the guide plate towards its outer edge and are thrown out, which is the first acceleration. Then, the throwed particles collide with the impact plate installed on the rotor body at an appropriate angle, which is the second acceleration, allowing the particles to obtain greater impact crushing energy at lower rotor speeds.

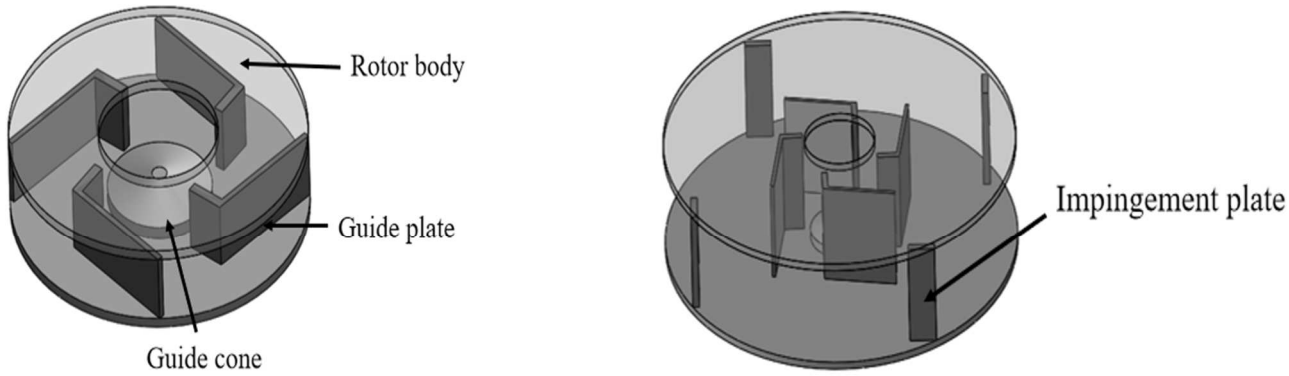

Fig. 1 *Schematic diagram of rotor structure*

The structural design of the secondary acceleration type rotor is mainly reflected in the impact plate. In traditional rotors, particles are only accelerated once by the guide plate before colliding with the cutting board on the inner wall of the crushing chamber, so the kinetic energy obtained is relatively small. In the secondary acceleration type rotor, the particles are accelerated by the guide plate for the first time and then collide with the impact plate, resulting in secondary acceleration. The particles are accelerated twice in the crushing process and are able to obtain a large kinetic energy. In order to achieve secondary acceleration, to ensure that the particles accelerated by the guide plate can collide with the impact plate, this paper analyses the acceleration process of particles in the rotor according to kinematics theory, and theoretically determines the installation position and installation angle of the impact plate on the rotor body.

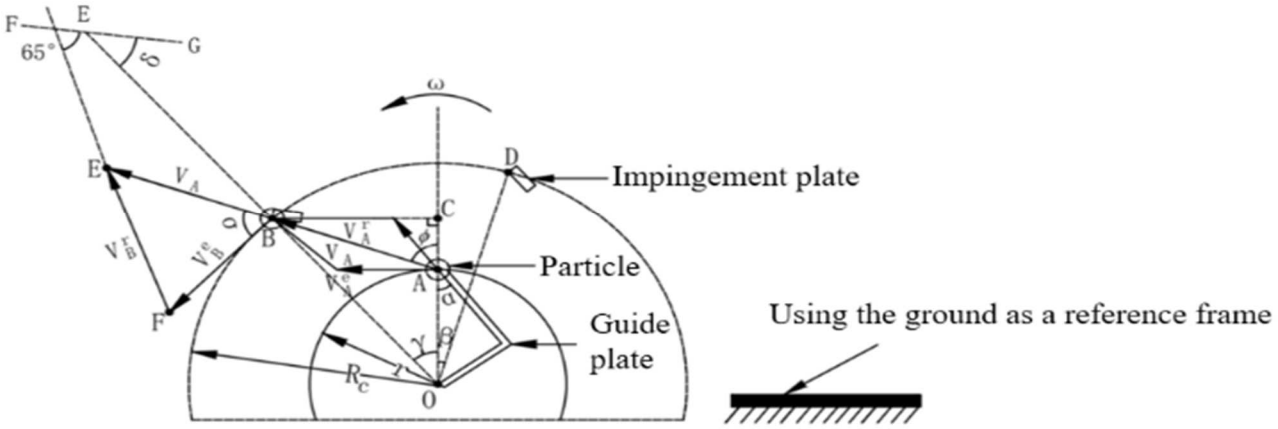

Fig. 2 *Analysis of the velocity of material particles*

The velocity analysis of particles in the secondary acceleration type rotor is shown in Figure 2. In the first acceleration process, the particles move along the guide plate to the end point *A* of the guide plate, and under the combined action of centrifugal force, extrusion force, and friction force, an acceleration is generated. They are thrown out from point *A* at a speed V_A. Among them, V_A is composed of the entanglement velocity V_A^e of particles at point *A* and the relative velocity V_A^r with the guide plate. After analysis, it can be concluded that equation (1):

$$\begin{cases} V_A{}^r = C_1 r\omega(\cos\alpha + f\sin\alpha) \\ V_A{}^e = r\omega \\ V_A = \sqrt{(V_A{}^r\cos\alpha)^2 + (V_A{}^r\sin\alpha + V_A{}^e)^2} = C_2 r\omega \end{cases} \quad (1)$$

$$C_1 = (1+f^2)^{1/2} - f$$

$$C_2 = \sqrt{C_1{}^2\cos^2\alpha + fC_1{}^2\sin 2\alpha + C_1{}^2 f^2\sin^2\alpha + C_1\sin 2\alpha + 2f\sin^2\alpha + 1}$$

Where:

V_A…The absolute velocity of particles at point A [m/s],

r…The inner radius of the rotor [mm],

ω…The rotor speed [r/min],

a…The installation angle of the guide plate [deg],

f…The friction coefficient between the material and the guide plate.

During the secondary acceleration process, the particles are thrown out by the guide plate and move from point A to point B at a speed of V_A. At point *B*, they should collide with the impact plate at an appropriate angle to achieve a good secondary acceleration effect. In Figure 2, *BE* is the extension line of *OB*, and *FG* is a straight line parallel to the impact plate. Let the motion time of particles from point *A* to point *B* be *t*. As shown in Figure. 2, the impact plate and rotor rotate together with an angular velocity ω during the time period *t*, turning over an angle of ($\beta + \gamma$). In order to obtain greater kinetic energy when particles collide with the impact plate, equation (2) should be satisfied:

$$\begin{cases} AC = V_A t\cos\varphi = R_c\cos\gamma - r \\ BC = V_A t\sin\varphi = R_c\sin\gamma \\ \gamma + \beta = \omega t \end{cases} \quad (2)$$

Solving equation (2) yields:

$$\gamma = \arccos\frac{r + \sqrt{r^2 - (1+\cot^2\varphi)(r^2 - R_c{}^2\cot^2\varphi)}}{R_c(1+\cot^2\varphi)} \quad (3)$$

$$\beta = \frac{180R_c\sin\gamma}{C_2\pi r\sin\varphi} - \gamma \quad (4)$$

Where:

R_c…The installation radius of the impact plate [mm],

γ…The angle between *OB* and radial (*OC*) [deg],

β…The angle at which the installation position of the impact plate lags behind the guide plate [deg],

φ…The angle between V_A and radial (*OA*) [deg].

Based on the geometric relationship in ΔABC in Figure 2, it can be concluded that:

$$V_A \sin\varphi = V_A{}^r \sin\alpha + V_A{}^e \tag{5}$$

Solving equation (5) yields:

$$\varphi = \alpha + \arcsin\frac{\sin(\frac{\pi}{2}-\alpha)}{C_1} \tag{6}$$

Research has shown that when the relative velocity $V_B{}^r$ of the particles at point B and the rotor speed ω are unchanged, in order to obtain a better acceleration of the material, the recovery coefficient of the particles and the impact plate should be chosen as a larger value [11]. Therefore, the incident angle of the particles is selected as 65° to achieve a larger recovery coefficient.

In $\triangle BEF$, it is obtained through the cosine theorem of triangles that:

$$\delta = \arcsin\frac{C_2 r\sin\sigma}{\sqrt{R_c{}^2 + C_2{}^2 r^2 - 2C_2 R_c r\cos\sigma}} - 25 \tag{7}$$

Where:

δ…The installation angle of the impact plate [deg],

σ …The angle between V_A and $V_B{}^e$ [deg],

$V_B{}^e$ …The entanglement velocity of material particles at point B [m/s].

From the above analysis, it can be concluded that the lag angle of the impact plate β and installation angle δ are not related to the angular velocity of the rotor, but only to the inner radius r, outer radius R, and installation angle of the guide plate of the rotor a and the friction coefficient f between the particle and the guide plate is related.

Taking the traditional rotor of PL840 vertical shaft impact crusher as an example, referring to the existing structure, the outer radius of the rotor R=400mm and the inner radius of the rotor r=200mm are taken. The impact plate is installed on the rotor, and the installation radius of the impact plate should be smaller than the outer radius R of the rotor. So taking the installation radius R_c=370mm. As can be seen from Figure. 2, the mounting position of the impact plate can be determined by the lag angle of the impact plate β and the installation radius R_c. With reference to the existing structure (guide plate installation angle a = 42.5°, splitting cone inclination angle θ = 15°), the friction coefficient between the particle and the guide plate f = 0.3 was determined by experimental method [15]. Substitute the above values into equations (5) and (6) to obtain the lag angle of the impact plate β= 6.3°, installation angle of impact plate δ= 26.8°.

Based on the calculated data parameters, the traditional rotor of the PL840 vertical shaft impact crusher is improved to a secondary acceleration type rotor. As shown in Figure 3 (a), the rotor body is composed of a rotor upper plate, a rotor lower plate, and four guide plates. The rotor lower plate has grooves for welding impact plates and installing throwing head, and the rotor upper plate has through holes for installing throwing head and impact plates. The section view of the assembled secondary acceleration rotor is shown in Figure 3 (b).

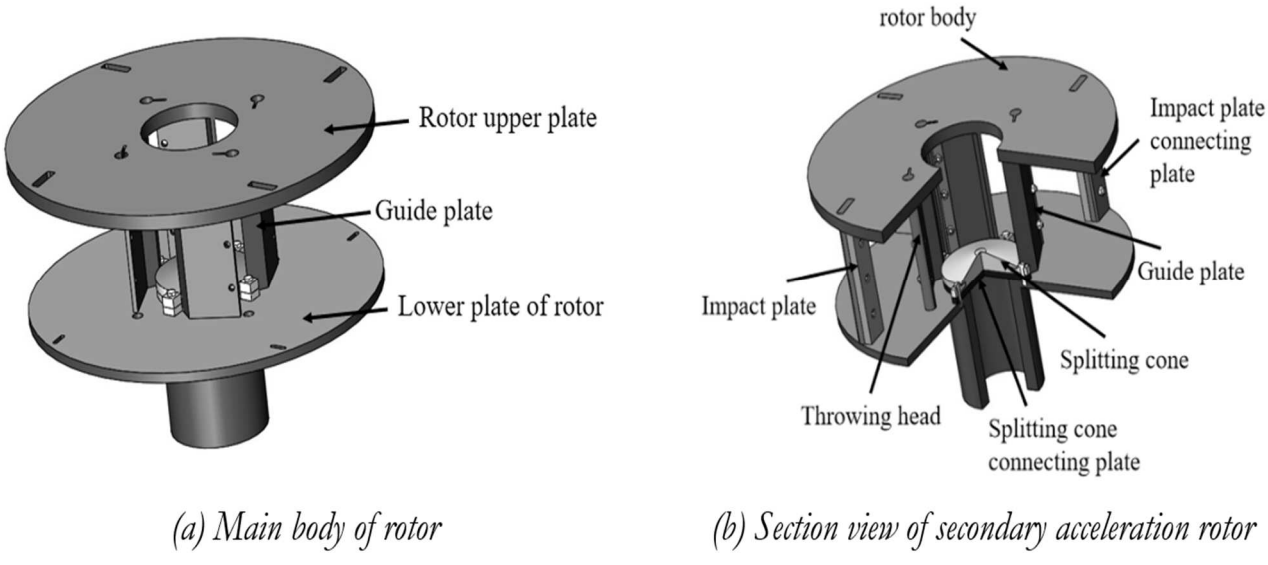

(a) Main body of rotor *(b) Section view of secondary acceleration rotor*

Fig. 3 *Secondary acceleration type rotor structure*

3 Gas solid coupling analysis method for material acceleration effect

During the operation of the vertical shaft impact crusher, particles are subjected to multiple impacts and collisions from the throwing head, impact plate, and other particles in the crushing chamber. During the impact, grinding, and crushing process, air disturbance occurs, generateing gas-solid two-phase flow movement. In order to analyze the secondary acceleration effect of the designed rotor, this paper adopts the gas-solid two-phase flow coupling method to calculate and analyze the motion process of the particle in the crushing chamber, the collision position of the particle in the crushing chamber, and the average throwing speed of the rotor.

The rotor in the crushing chamber undergoes rotational motion, and the *RNG k-e* turbulence model can be used to simulate the flow field in the crushing chamber. The *RNG k-e* model takes into account the effect of rotating flow on turbulence in mean motion, and by correcting the turbulent viscosity coefficients, it can better deal with flow problems with high strain rates and large degree of streamline curvature [16-17]. The control equation of *RNG k-e* turbulence model can be represented by the following equation [18-20]:

If gas is incompressible, then the *k* equation is:

$$\frac{\partial \rho k}{\partial t}+\frac{\partial\left(\rho U_j k\right)}{\partial x_j}=-\frac{2}{3}\rho k\frac{\partial u_k}{\partial x_k}+\frac{\partial}{\partial x_j}\left(\frac{\mu_{eff}}{\sigma_k}\frac{\partial k}{\partial x_j}\right)+G_k-\rho\varepsilon d \tag{8}$$

Equation *e*:

$$\frac{\partial \rho\varepsilon}{\partial t}+\frac{\partial\left(\rho U_j \varepsilon\right)}{\partial x_j}=-[(\frac{2}{3}C_{\varepsilon 1}-C_{\varepsilon 3}+\frac{2}{3}C_\mu C_\eta\frac{k\partial u_k}{\varepsilon\partial x_k})\rho\varepsilon\frac{\partial u_k}{\partial x_k}+\frac{\partial}{\partial x_j}(\frac{\mu_{eff}}{\sigma_\varepsilon}\frac{\partial_\varepsilon}{\partial x_j})]+\rho\frac{\varepsilon}{k}[(C_{\varepsilon 1}-C_\eta)G_k-C_{\varepsilon 2}\rho\varepsilon] \tag{9}$$

Where:

ϱ…The gas density,

k…The turbulent kinetic energy,

ε…The turbulent energy dissipation rate,

$C_{\varepsilon 1}$=1.42, $C_{\varepsilon 2}$=1.68, β=0.015, C_u=0.085, η_0=4.25, $\eta=SK/\varepsilon$, $C_n=\frac{\eta(1-\eta/\eta_0)}{1+\beta\eta^3}$, $S=\sqrt{2\overrightarrow{S_{ij}}\overrightarrow{S_{ij}}}$,

$C_{\varepsilon 3}=[-1+-2C_{\varepsilon 1}-3m_1(n-1)+(-1)^\delta\sqrt{6}C_\mu C_\eta\eta]/3$.

To describe the motion state of particles in a crushing chamber using the discrete element method, it is necessary to first determine the contact model between the particles and the boundary, in order to accurately calculate the force between the particles and the boundary. In the study, the particle model is simplified accordingly, ignoring the plastic deformation caused by the contact between particles and between particles and the crushing chamber wall. It is also set that the contact between each other belongs to inviscid contact, and its contact mechanics model conforms to the Hertz-Mindlin no-slip contact model [6, 21, 22], so this contact model is chosen to describe the contact collision between particles and particles, and particles with the rotor body and particles with the crushing chamber wall surface.

The key to simulating the motion state of particles in the flow field with EDEM lies in determining the contact force after particle collision. Assuming that two spherical particles with radii r_1 and r_2 collide at velocities v_1 and v_2, the normal overlap x can be expressed as:

$$\chi=r_1+r_2-\left|\overrightarrow{r_1}-\overrightarrow{r_2}\right| \tag{10}$$

Where:

$\overrightarrow{r_1}$, $\overrightarrow{r_2}$…The position vectors of the two ball centers, respectively.

The wall surface of the crushing chamber can be regarded as consisting of a number of spherical particles, so that the equivalent spherical particle radius r^* is:

$$r^*=\frac{r_1 r_2}{r_1+r_2} \tag{11}$$

The combined force achieved by the inter-particle collision can be found by superposing the normal contact force F_n and tangential contact force F_t operation. The formula for the normal contact force between particles is shown in equation (12):

$$\begin{cases} F_n=\frac{4}{3}E^*\sqrt{E^*\chi^3} \\ E^*=\frac{1-v_1^{\,2}}{E_1}+\frac{1-v_2^{\,2}}{E_2} \end{cases} \tag{12}$$

Where:

E^*…The equivalent elastic modulus,

E_1, E_2…The elastic moduli of two spherical particles, respectively.

The formula for tangential contact force between particles is shown in equation (13):

$$\begin{cases} F_t=-S_t\delta \\ S_t=8G^*\sqrt{r^*\chi} \\ G^*=\frac{2-v_1^{\,2}}{G_1}+\frac{2-v_2^{\,2}}{G_2} \end{cases} \tag{13}$$

Where:

δ…The normal overlap of spherical particles,

S_t…The tangential stiffness of particles,

G^*…The equivalent shear modulus,

G_1, G_2…The shear moduli of two spherical particles, respectively.

For the coupled calculation of the flow field in the crushing chamber, there is a particle phase in the gas phase.

When using the Eulerian-Eulerian method to simulate the motion of the flow field in a crushing chamber, it is necessary to add the calculation of void fraction to the fluid control equation, and the mathematical expression is shown in equation (14) [23-24]:

$$\frac{\partial}{\partial t}(\varepsilon\rho_g\varphi)+div(\varepsilon\rho_g\vec{u}\varphi)=div(\Gamma\varepsilon grad\varphi)+S \tag{14}$$

In the above equation, from left to right respectively represent the transient term, convection term, diffusion term, and source term, and the expanded expression is as follows:

$$\begin{aligned}&\frac{\partial}{\partial t}(\varepsilon\rho_g\varphi)+\frac{\partial}{\partial x}(\varepsilon\rho_g u\varphi)+\frac{\partial}{\partial y}(\varepsilon\rho_g v\varphi)+\frac{\partial}{\partial z}(\varepsilon\rho_g w\varphi)=\\&\frac{\partial}{\partial x}[\Gamma\varepsilon\frac{\partial\varphi}{\partial x}]+\frac{\partial}{\partial y}[\Gamma\varepsilon\frac{\partial\varphi}{\partial y}]+\frac{\partial}{\partial x}[\Gamma\varepsilon\frac{\partial\varphi}{\partial z}]+S\end{aligned} \tag{15}$$

Where:

φ…A universal variable,

u, v, w, t …Solving variables,

Γ…The generalized diffusion coefficient,

S…The generalized source term.

Due to the fact that the simulation of the flow field in the crushing chamber belongs to the case of dense particles and the particle density is much higher than the air density [25]. In the gas-solid coupling calculation of the flow field in the crushing cavity, the Eulerian-Eulerian method is used to simulate the interaction, except for the drag force, other forces are very small and can be ignored, so in this paper, the drag force model is used to simulate the drag force of the gas on the particles in the crushing cavity. When using the Ergun and Wen&Yu drag model to calculate the drag force F_d of the gas in the crushing chamber on particles, the drag force expression is related to the gas fraction, as shown in equation (16) [17, 26]. When the volume fraction ε_g occupied by the gas phase in the crushing chamber is less than or equal to 0.08, the magnitude of the trailing force is independent of the particle Reynolds number R_{es}; When the volume fraction ε_g occupied by the gas phase in the crushing chamber is greater than 0.08, there exists a certain relationship between the magnitude of the trailing force of the gas on the particles and the Reynolds number R_{es} of the particles.

$$\begin{cases}F_d=150\dfrac{\varepsilon^2\mu_g}{\varepsilon_g d_p{}^2}+1.75\dfrac{\rho_g\varepsilon_s\left|\vec{v_s}-\vec{v_g}\right|}{d_p}, & \varepsilon_g\le 0.08\\ F_d=0.75C_D\dfrac{\rho_g\varepsilon_s\varepsilon_g\left|\vec{v_s}-\vec{v_g}\right|}{d_p}\varepsilon_g{}^{-2.65}, & \varepsilon_g>0.08\end{cases} \tag{16}$$

When the volume fraction ε_g of the gas phase is greater than 0.08 and the particle Reynolds number is less than 1000, the calculation formula for the gas resistance coefficient C_D is shown in equations (17) and (18). When the Reynolds number is greater than or equal to 1000, the gas resistance coefficient is a constant, with C_D=1.44.

$$C_D=\frac{24}{\varepsilon_g\,\mathrm{Re}_s}\left[1+0.15\left(\varepsilon_g\,\mathrm{Re}_s\right)^{0.687}\right] \tag{17}$$

$$\mathrm{Re}_s=\frac{\rho_g d_p\left|\vec{v_s}-\vec{v_g}\right|}{\mu_g} \tag{18}$$

Where:

ε_g, ε_s…The volume fraction of gas phase and particle phase in the crushing chamber, respectively,

μ_g…The the viscosity coefficient of the gas phase,

ϱ_g…The gas phase density; d_p represents the particle diameter,

v_g, v_s…The velocities of the gas phase and particles, respectively.

The gas-solid coupling solution process for the flow field in the crushing chamber is shown in Figure 4. Firstly, FLUENT iterates the flow field of the crushing chamber within one time step to convergence, and then converts the flow field data into the drag force acting on the particles by gas through a drag model, which is transmitted to EDEM; At this point,

EDEM starts the time step calculation, simulating the motion of particles in the crushing chamber, calculating external forces such as particle collision force, calculating particle acceleration through Newton's second law, and integrating time to obtain the velocity and position of each particle; Finally, EDEM transfers the particle information to FLUENT in the form of momentum sinks for the next time step calculation, and so on.

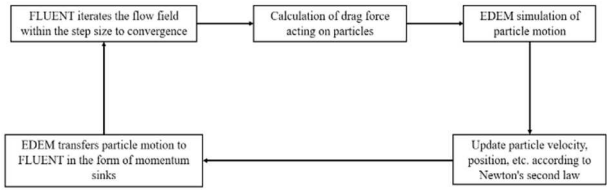

Fig. 4 *Gas solid coupling solution flowchart*

4 Establishment and verification of a simulation model for particle acceleration effect

4.1 Establishment of simulation model for particle acceleration effect

Since the solid-phase model imported into EDEM has to be coupled with the gas-phase model for calculations, and FLUENT flow field calculations require high mesh quality for the gas-phase model. Therefore, without affecting the simulation results, simplify the assembly relationship of the solid phase model's structures such as the dividing cone, throwing head, and impact plate accordingly. In order to facilitate observation, the diameter of the rotor upper plate has been reduced. Set the inner radius of the rotor to r=200 mm, the outer radius to R=400 mm, and the splitting cone inclination angle θ= 15°, installation angle of guide plate a= 42.5°, impact plate lag angle β= 6.3° and installation angle δ= 26.8°.

Select the multi coordinate reference model MRF in FLUENT to simulate the movement of gas in the rotating region and establish a flow field model in the crushing chamber. The simulation model for material acceleration effect established is shown in Figure 5. The selected material for the particles is limestone. Due to the fact that in actual production, the particles processed by the vertical shaft impact crusher are mostly produced by the previous process, which meets certain particle size requirements, this article uses a spherical particle model with a diameter of 40mm in simulation. The outer cylindrical grid in Figure 5 is the data collection area. In order to more accurately collect the velocity of particles after being accelerated, it is necessary to reasonably set the parameters of the data collection area in the flow field. Due to the improved rotor outer diameter R2=800 mm, in order to enable the data collection area to only collect the throwing speed of the rotor without collecting the velocity of particles at other positions inside the rotor, the inner diameter and outer diameter of the data collection area were set to 800mm and 1100mm in the simulation.

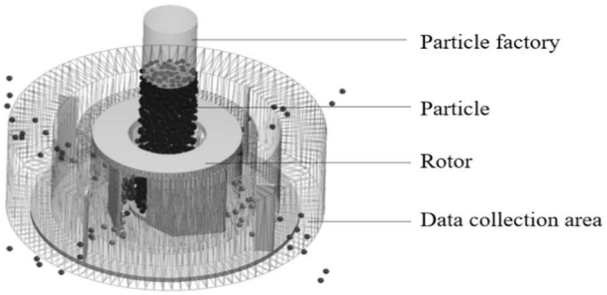

Fig. 5 *Simulation model of material acceleration effect*

4.2 Verification of simulation model for particle acceleration effect

Verify the reliability of the particle acceleration effect simulation model by examining whether the theoretical value of crushing force is consistent with the simulation calculation results of crushing force [27].

4.2.1 Theoretical calculation of crushing force

Calculate the crushing force of an impact crusher based on the momentum theorem:

$$P = \frac{m_1 m_2}{m_1 + m_2} \frac{V}{t} \tag{19}$$

Where:

V…The particle impact velocity [m/s],

t…The impact time [s],

m_1…The quality of limestone [kg],

m_2…The quality of the cutting board [kg].

The particle impact velocity V can be calculated by formula (20) [28]:

$$V = K_V \sqrt{\frac{1}{\delta}} \frac{\sigma^{5/6}}{E_1^{1/3}} \tag{20}$$

Where:

K_v…The impact velocity coefficient; δ is the density of the material particles [kg/m^3],

σ…The compressive strength of material particles [Pa].

The impact time t refers to the duration from the initial contact between material particles and the cutting board to the occurrence of crushing, calculated using equation (21). This formula is consistent with the crushing time determined by recording and analyzing the crushing process through high-speed photographic film [27-29].

$$t = \frac{2.7 r_1}{V^{\frac{1}{5}}} \left(\frac{\delta}{E_1}\right)^{\frac{2}{5}} \tag{21}$$

4.3 Simulation analysis of crushing force

Establish a simulation model of an R = 800 mm vertical axis impact crusher in EDEM and set the physical parameters of the particles. Through simulation experiments on a single particle crushing model, the force variation curve of the cutting board with time is obtained, as shown in Figure 6.

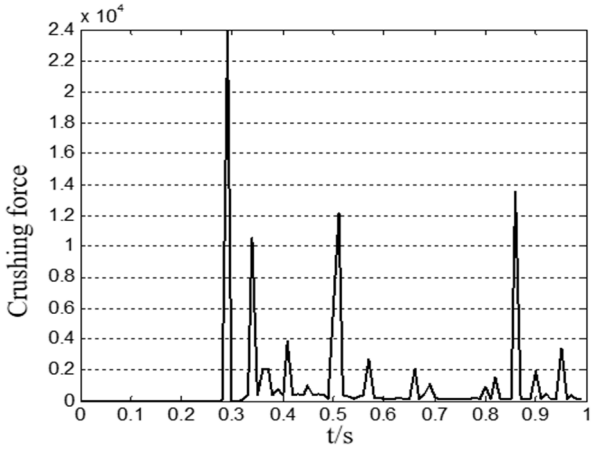

Fig. 6 *Cutting board force diagram during single particle simulation*

From Figure 6, it can be seen that the maximum force acting on the cutting board is 23846N. As the crushing force on the particles is a pair of interacting forces with the cutting board, it can be considered that the maximum crushing force on the particles is 23846 N. Through three simulations and calculations, it was found that the average maximum crushing force of particles is 22977 N, which is basically consistent with the maximum crushing force calculated through theoretical formulas of 22461 N. Therefore, it can be considered that the setting of inter particle bonding parameters and simulation physical parameters in the crushing model is reasonable, that is, the simulation model can simulate the crushing process of real particles.

5 Simulation analysis of the operating effect of a secondary acceleration type rotor

5.1 Analysis of particle motion process

Using the established particle acceleration simulation model to analyze the motion trajectory of individual particles and the motion process of particle groups in the crushing chamber. The outer diameter of the secondary acceleration type rotor is R_2=800mm. In practical applications, the traditional vertical shaft impact crusher rotor with a diameter of 800mm has a speed range of 800-1800r/min. However, higher rotor speeds will increase the impact force when particles come into contact with the cutting board, exacerbate the wear of easily worn parts such as the cutting board and guide plate, and cause particle crushing to be too fine and forming particle size to be poor. So, during the simulation process, the rotor speed was set to 1200 r/min. Reference [6] sets parameters such as Poisson's ratio, density, shear modulus, friction coefficient, and collision recovery coefficient for particles and rotor materials.

The motion trajectory of a single particle is shown in Figure 7 (a). It can be seen from the Figure 7 that the turning points of the motion trajectory of a single particle indicate collision with the guide plate, impact plate, and impact board in sequence. Overall, the collision acceleration process of particles is mainly reflected at the guide plate, impact plate, and crushing chamber impact plate, corresponding to regions A, B, and C in Figure 7 (b), respectively. Through simulation experiments, it was found that the collision acceleration regions of different particle sizes under different working conditions are similar to Figure 7 (b). From Figure 7(b), it can be seen that the particle group is accelerated by the guide plate to form a material flow, which collides with the impact plate again to produce secondary acceleration, and finally collides with the anvil plate installed in the crushing chamber to achieve crushing.

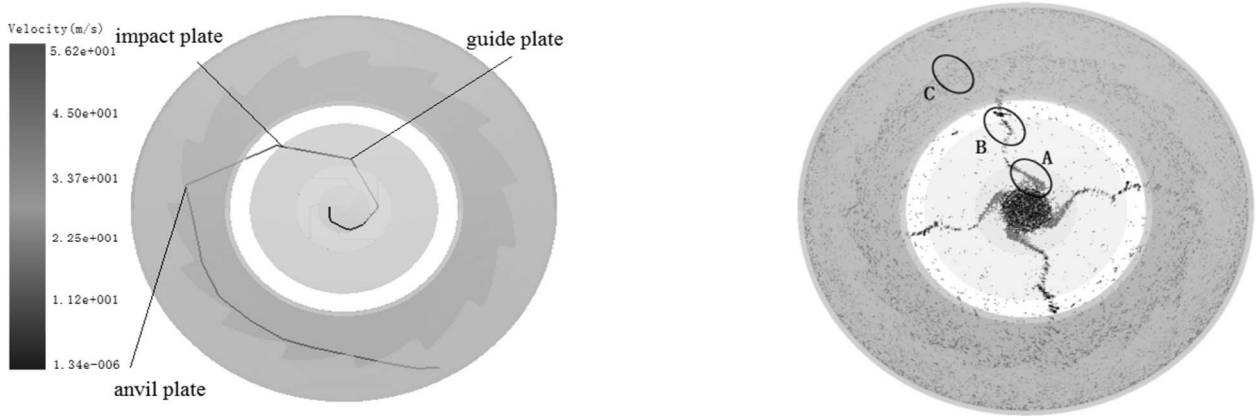

(a) The motion trajectory of a single particle *(b) Particle swarm collision area*

Fig. 7 *Movement process of material in crushing chamber*

The main acceleration collision positions of particles in the crushing chamber are shown in Figure 8. Hide the outer shell of the crushing chamber and the rotor body to display the particles in vector state. The color of the particles increases from blue to red, indicating a gradual increase in speed. Arrows indicate the velocity direction of particles. The particles fall into the rotor body along the direction of gravity, and after being accelerated by the guide plate, the color of the particle velocity changes from blue to green (Speed increase), causing the particles to generate a certain amount of impact energy. During this collision acceleration process, a small amount of particles will be broken. After the particles are accelerated and collided by the impact plate, the colour of the particles' speed changes from green to red (speed increase), which provides the particles with kinetic energy to collide with the anvil, and this collision is also accompanied by a small amount of particles' crushing. The final crushing of particles is mainly achieved by collision with the cutting board. During the collision with the cutting board, the stored kinetic energy of the particles is instantly released, generating a huge crushing force. As a result, the color of the particle velocity changes from red to blue (the velocity decreases), and the direction of velocity also changes significantly. Some particles that have not fully released their kinetic energy continue to collide with other particles in the crushing chamber to achieve fragmentation.

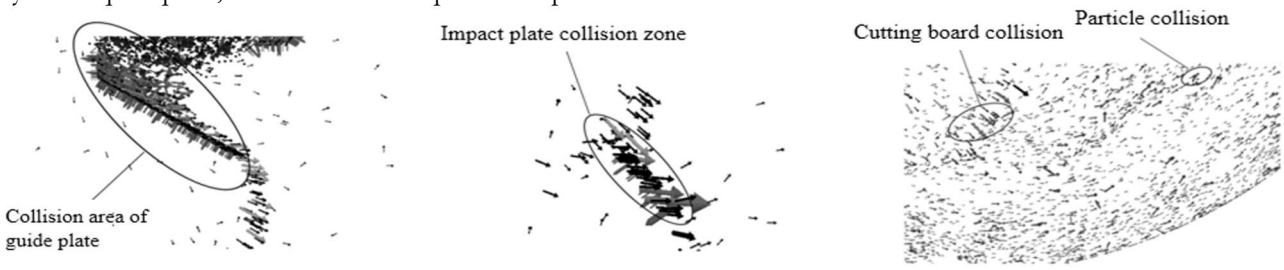

Fig. 8 *Collision position of particles in the crushing chamber*

In order to verify the superiority of the secondary acceleration type rotor in terms of material acceleration effect, a blue collection area is set on the collision surface between the impact plate and the particle, as shown in Figure 9. By counting the number of particles passing through the collection area, the number of particles subjected to secondary acceleration is calculated to further verify the reliability of the secondary acceleration rotor for particle secondary acceleration. In order to avoid the impact of particles overflowing above the rotor inlet directly colliding with the impact plate and rebounding from the crushing chamber cutting board, and the impact of particles colliding with the impact plate again on statistical data, it is necessary to set certain restrictions on the particles in contact and collision with the impact plate. Since the particles overflowing from above the rotor inlet are not in contact with the guide plate, they are not accelerated by the guide plate, resulting in lower speeds for such particles when they come into contact with the impact plate. After the latter collides with the cutting board, there is a significant loss of kinetic energy and a relatively low speed. To eliminate the influence of these two types of particles on the data collection area, the collection area is set to only record information on particles with a speed of 25m/s or above. Through simulation, the curve of the number of particles passing through the collection area over time is obtained, as shown in Figure 10.

In Figure 10, the number of particles passing through the collection zone is 30,328, while the total number of particles generated is 39,082. It is calculated that roughly 77.6% of the particles can collide with the impact plate, so that the particles can obtain a larger impact velocity. The design requirements of the secondary accelerated rotor are met.

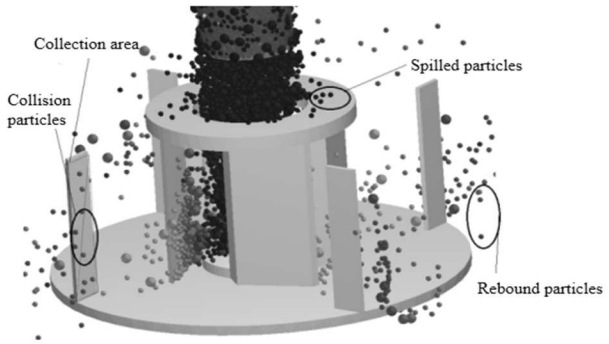

Fig. 9 *Impact plate acquisition model*

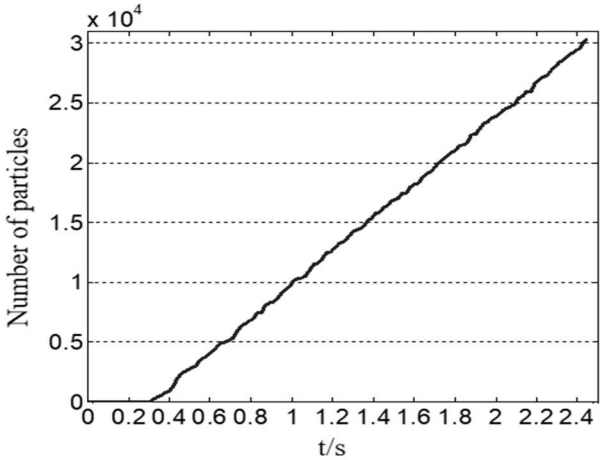

Fig. 10 *Impact plate acquisition model*

5.2 Particle acceleration effect analysis

The outer diameter of the secondary acceleration type rotor is R_2=800 mm, and the rotor speed is set to 1200r/min. Set the feeding speed to 25 Kg/s and the simulation time to 2s. The velocity of the collected particles is exported from the post-processing module, and then the average value of the velocity data of this test is obtained, which is the average throwing velocity. The acceleration effect on particles as a function of time for the conventional rotor and the secondary acceleration type rotor is shown in Figure 11.

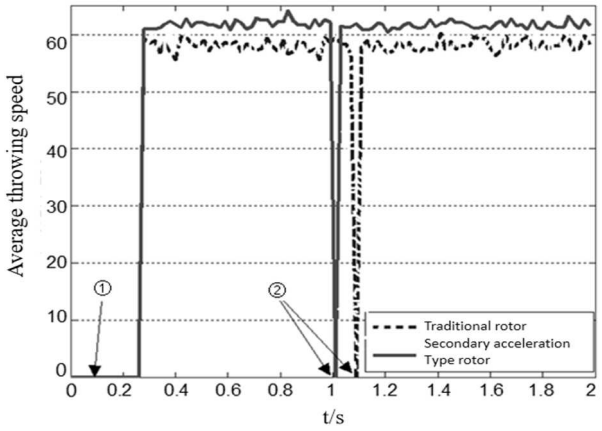

Fig. 11 *Acceleration effect over time curve*

In Figure 11, it can be seen from ① that the velocity of particles was 0 before approximately 0.3 seconds, because no particles entered the data collection area before 0.3 seconds. After 0.3 seconds, as shown in ②, there was a phenomenon of particle velocity being 0 at certain moments in the acceleration process simulation curve. As mentioned earlier, this is because there are no particles in the data collection area within this time step, and the speed data of the particles cannot be collected in the data collection area, which does not mean that the speed of the particles in the data collection area is 0 at that time. In order to make the calculations more realistic and reliable, this test programme has removed the point where the velocity is 0 when calculating the average throwing velocity of the particles. After calculation, the average throwing speed of the traditional rotor was ultimately determined to be 57.14m/s, while the average throwing speed of the improved design of the secondary acceleration type rotor was 60.89m/s. Compared with traditional rotors, the average throwing speed of the secondary acceleration type rotor has increased by about 6%, meeting the design requirements.

6 Conclusion

Based on the kinematic analysis of the particles thrown from the throwing head, the design method of the secondary acceleration type rotor is proposed. The mounting position of the impact plate is on the helix of the particle flight, which is co-located by the lag angle θ and the mounting radius R of the impact plate.

A gas-solid coupling simulation model of the effect of rotor on particle acceleration was established and the motion process of particles in the crushing chamber and the collision position of particles in the crushing chamber were calculated and analysed by CFD-EDM method. Research results show that roughly 77.6 % of the material in the crushing chamber is accelerated twice by the rotor.

The analysis of the average throwing speed of the secondary accelerated rotor shows that the average throwing speed of the traditional rotor is 57.14 m/s, and the average throwing speed of the designed secondary accelerated rotor is 60.89 m/s. The average throwing speed of the secondary accelerated rotor is increased by about 6% compared with the traditional rotor.

Acknowledgement

This work was financially supported by The National Natural Science Foundation of China (No.52065007).

References

[1] AL-KHASAWNEH, Y., Development and testing of a novel mathematical-physical model for the design of ring armor for the vertical shaft impact crushers. *Minerals Engineering*. 2021.

[2] KE SUN, LIMEI ZHAO, QITAO LONG. Optimization of Process Parameters for a Vertical Shaft Impact Crusher through the CFD-DEM Method. *Manufacturing Technology*. 2024.

[3] ARTYUKHOV, A., J. KRMELA, V. KRMELOVA. Manufacturing of Vortex Granulators: Simulation of the Vortex Fluidized Bed Functioning under the Disperse Phase Interaction in the Constrained Motion. *Manufacturing Technology* 2020, 20(5): 547-53.

[4] LAZI V , ARSI D , NIKOLI R .Reparation by Hard Facing of the Damaged Secondary Stone Crushers[J]. *Manufacturing Technology*, 2016, 16(2):375-380.

[5] SEGURA-SALAZAR, J.; BARRIOS, G. P.; RODRIGUEZ, V.; TAVARES, L. M., Mathematical modeling of a vertical shaft impact crusher using the Whiten model. *Minerals Engineering* 2017.

[6] CANHUI, W.; LIMEI, Z.; ZHEN, C., Collision Energy Analysis within the Vertical Shaft Impact Crusher Based on the Computational Fluid Dynamics-Discrete Element Method. *ACS Omega*. 2024.

[7] DJORDJEVIC, N.; SHI, F. N.; MORRISON, R. D., Applying discrete element modelling to vertical and horizontal shaft impact crushers. *Minerals Engineering*. 2003.

[8] FANG, H.; YANG, J.; SONG, Y.; HUANG, W.; CHEN, J., Simulation and experimental study on the stone powder separator of a vertical shaft impact crusher. *Advanced Powder Technology*. 2020.

[9] YAQOUB, A.-K., Novel design modeling for vertical shaft impactors. *Powder Technology*. 2023.

[10] ZANDEN, H. V. D.; ZANDEN, M. V. D.; ZANDEN, R. V. D., The SynchroCrusher - Determinism versus chaos. A*T: Aufbereitungs-Technik*. 2002. (43-10).

[11] LI, S. Research on secondary acceleration type vertical shaft impact crushing tester. University of Jinan, 2015.

[12] CLEARY, P. W.; DELANEY, G. W.; SINNOTT, M. D.; CUMMINS, S. J.; MORRISON, R. D., Advanced comminution modelling: part 1 – crushers. *Applied Mathematical Modelling*. 2020.

[13] GRUNDITZ, S.; ASBJÖRNSSON, G.; HULTHÉN, E.; EVERTSSON, M., Fit-for-Purpose VSI Modelling Framework for Process Simulation. *Minerals*. 2020.

[14] DA CUNHA, E. R.; DE CARVALHO, R. M.; TAVARES, L. M., Simulation of solids flow and energy transfer in a vertical shaft impact crusher using DEM. *Minerals Engineering*. 2013.

[15] ANDRÉ, F. P.; TAVARES, L. M., Simulating a laboratory-scale cone crusher in DEM using polyhedral particles. *Powder Technology*. 2020.

[16] DON DASUN, A.; FABIAN, S.; SHREYAS, K.; ANDREA, D.; ALBA, D.-A.; BEREND VAN, W., Review of Modelling of Pyrolysis Processes with CFD-DEM. Flow, *Turbulence and Combustion*. 2023.

[17] FULLMER, W. D.; MUSSER, J., CFD-DEM solution verification: Fixed-bed studies. *Powder Technology*. 2018.

[18] JORDAN, M.; ANN, S. A.; WILLIAM, D. F.; OSCAR, A.; JOHN, B. B.; JOHANNES, B.; KEVIN, G.; ANDREW, M.; ROBERTO, P.; DEEPAK, R.; MICHELE, R.; WEIQUN, Z.; MADHAVA, S., MFIX-Exa: A path toward exascale CFD-DEM simulations. *The International Journal of High Performance Computing Applications*. 2021.

[19] KERST, K.; ROLOFF, C.; MEDEIROS DE SOUZA, L. G.; BARTZ, A.; SEIDEL-MORGENSTERN, A.; THÉVENIN, D.; JANIGA, G., CFD-DEM simulations of a fluidized bed crystallizer. *Chemical Engineering Science*. 2017.

[20] KURUNERU, S. T. W.; MARECHAL, E.; DELIGANT, M.; KHELLADI, S.; RAVELET, F.; SAHA, S. C.; SAURET, E.; GU, Y., A Comparative Study of Mixed Resolved–Unresolved CFD-DEM and Unresolved CFD-DEM Methods for the Solution of Particle-Laden Liquid Flows. *Archives of Computational Methods in Engineering*. 2018.

[21] COETZEE, C. J., Calibration of the discrete element method and the effect of particle shape. *Powder Technology*. 2016.

[22] DONGXU, Y.; JIANQUN, Y.; YANG, W.; LONG, Z.; YE, T.; NA, Z., Soil Particle Modeling and Parameter Calibration Based on Discrete Element Method. *Agriculture*. 2022.

[23] TONI EL, G.; BRUNO, B., Solid-liquid rotary kilns: An experimental and CFD-DEM study. *Powder Technology*. 2023.

[24] TONI EL, G.; SHAHAB, G.; BRUNO, B., Toward High-Order CFD-DEM: Development and Validation. I*ndustrial & Engineering Chemistry Research*. 2023.

[25] ZHAO, H.; ZHAO, Y., CFD-DEM simulation of pneumatic conveying in a horizontal channel. *International Journal of Multiphase Flow*. 2019.

[26] ZHAO, H.; ZHAO, Y., CFD-DEM simulation of pneumatic conveying in a horizontal pipe. *Powder Technology*. 2020.

[27] JIN, C.; FENG, X.; ZHANG, C., Application of neural network to back analysis of mechanical parameters of columnar joint basalt. *Journal of Hydroelectric Engineering*. 2010.

[28] ZENG, H.; ZHOU, E., Determination of impact speed, impact time and crushing force of impact crusher. *Mining machinery*. 1994, (1), 5.

[29] LEWINSKI, J.; MAZELA, A., Experimental Analysis of Impact Comminution Phenomena in a Model Impact Crusher. 1984.